Biochemical and Biophysical Research Communications 462 (2015) 27–32

Contents lists available at ScienceDirect

Biochemical and Biophysical Research Communications

journal homepage: www.elsevier.com/locate/ybbrc

Application of dynamic metabolomics to examine *in vivo* skeletal muscle glucose metabolism in the chronically high-fat fed mouse

Greg M. Kowalski [a, *], David P. De Souza [c], Micah L. Burch [b], Steven Hamley [a], Joachim Kloehn [c], Ahrathy Selathurai [a], Dedreia Tull [c], Sean O'Callaghan [c], Malcolm J. McConville [c], Clinton R. Bruce [a]

[a] Centre for Physical Activity and Nutrition Research, School of Exercise and Nutrition Sciences, Deakin University, Burwood, Victoria 3125, Australia
[b] Brigham and Women's Hospital, Department of Medicine, Boston, MA, USA
[c] Metabolomics Australia, Bio21 Institute of Molecular Science and Biotechnology, University of Melbourne, Parkville, Victoria 3010, Australia

ARTICLE INFO

Article history:
Received 10 April 2015
Available online 28 April 2015

Keywords:
Muscle insulin resistance
Metabolomics
Stable isotopes

ABSTRACT

Rationale: Defects in muscle glucose metabolism are linked to type 2 diabetes. Mechanistic studies examining these defects rely on the use of high fat-fed rodent models and typically involve the determination of muscle glucose uptake under insulin-stimulated conditions. While insightful, they do not necessarily reflect the physiology of the postprandial state. In addition, most studies do not examine aspects of glucose metabolism beyond the uptake process. Here we present an approach to study rodent muscle glucose and intermediary metabolism under the dynamic and physiologically relevant setting of the oral glucose tolerance test (OGTT).

Methods and results: In vivo muscle glucose and intermediary metabolism was investigated following oral administration of [U-^{13}C] glucose. Quadriceps muscles were collected 15 and 60 min after glucose administration and metabolite flux profiling was determined by measuring ^{13}C mass isotopomers in glycolytic and tricarboxylic acid (TCA) cycle intermediates via gas chromatography–mass spectrometry. While no dietary effects were noted in the glycolytic pathway, muscle from mice fed a high fat diet (HFD) exhibited a reduction in labelling in TCA intermediates. Interestingly, this appeared to be independent of alterations in flux through pyruvate dehydrogenase. In addition, our findings suggest that TCA cycle anaplerosis is negligible in muscle during an OGTT.

Conclusions: Under the dynamic physiologically relevant conditions of the OGTT, skeletal muscle from HFD fed mice exhibits alterations in glucose metabolism at the level of the TCA cycle.

1. Introduction

Defects in muscle glucose metabolism, particularly insulin resistance, are a characteristic feature of obesity and type 2 diabetes [1]. Our current understanding of the mechanisms underlying muscle insulin resistance has been aided by rodent models, especially the high-fat diet (HFD) fed mouse. Accordingly, techniques to determine insulin sensitivity in humans, such as the 'gold standard' euglycemic hyperinsulinemic clamp, have been adapted to allow for detailed assessment of mouse glucose homeostasis [2–4]. The application of the clamp to rodent studies has yielded significant insight into the regulation of muscle insulin action, however, there are limitations associated with this method, including the fact that the clamp does not replicate the dynamic changes in circulating insulin, glucose and other hormones and metabolites that occur following nutrient ingestion. During a typical mouse clamp, glucose and insulin are infused directly into the systemic circulation via a peripheral vein, not the hepatic portal vein which is their natural route of entry into the body [5]. Moreover, studies largely focus on determining radioactive tracer-derived measures of muscle glucose uptake as the sole readout of glucose metabolism [3,4], without examining the metabolic fate of glucose once it has entered the myocyte. Studies are therefore required to examine how the presence of insulin resistance impacts on the pathways of glucose metabolism in muscle under conditions that better reflect the physiology of the postprandial state. The oral glucose tolerance test (OGTT) is used in clinical and laboratory investigations to assess

* Corresponding author. Centre for Physical Activity and Nutrition Research, School of Exercise and Nutrition Sciences, Deakin University, 221 Burwood Highway, Burwood, VIC 3125, Australia.
E-mail address: greg.kowalski@deakin.edu.au (G.M. Kowalski).

http://dx.doi.org/10.1016/j.bbrc.2015.04.096
0006-291X/

whole-body glucose metabolism. The OGTT has also been adapted for rodent studies and is now one of the most widely used physiological tests in mice [2]. However, unlike the clamp, the OGTT not only takes into account insulin sensitivity, but also other factors critical for regulating glucose homeostasis including insulin secretion and glucose effectiveness, and therefore more closely replicates physiological conditions [5]. Given the lack of data on muscle glucose metabolism in mice under these physiologically relevant conditions, the aim of this study was to integrate stable isotope methodology and targeted metabolomics to develop an approach to track the fate of glucose derived carbon through key metabolic pathways in muscle during an OGTT. Furthermore, we aimed to examine whether skeletal muscle glucose metabolism is altered in the obese, glucose intolerant HFD fed mouse.

2. Materials and methods

2.1. Animals

All experiments were approved by the Monash University Animal Research Platform Animal Ethics Committee and were in accordance with the National Health and Medical Research Council of Australia Guidelines on Animal Experimentation. Mice were maintained at 22 ± 1 °C on a 12 h light/dark cycle, with free access to food and water. Eight week old male C57BL/6 mice (Monash Animal Research Platform) were maintained on a standard chow control diet (9% energy as fat, Barastoc Rat and Mouse, Ridley AgriProducts, Melbourne, Australia) or high-fat diet (HFD; 42% energy from fat, 20% by weight from sucrose, Specialty Feeds SF4-001, Glen Forrest, WA, Australia) for 10 weeks.

2.2. Oral [U-^{13}C] glucose tolerance test

After a 5 h fast, mice underwent an OGTT where [U-^{13}C]-glucose (50 mg; 25% w/v; 99% enrichment, Sigma Aldrich) was administered via oral gavage. Quadriceps muscles were collected at 15 and 60 min following glucose administration and were rapidly frozen in liquid nitrogen. Blood (50 μl) was also collected at these time points via the tail vein and blood glucose was measured with a glucose meter (Accu-Check, Roche, NSW, Australia) and plasma insulin via rat/mouse ELISA (Millipore, St Louis, MO, USA) according to the manufacturer instructions.

2.3. Tissue metabolite extraction

Quadriceps muscle (10–20 mg) was weighed into cryomill tubes and 600 μL of 3:1 methanol:water (v/v) and 2 nmol scyllo-inositol (internal control) was added to each tube. Samples were extracted using a Precellys bead-mill with a Cryolys attachment (Bertin Technologies, France). The homogenate was transferred to a new tube, 150 μL chloroform added and the extract centrifuged. The supernatant was transferred to a new tube and 300 μL H_2O added followed by centrifugation. The upper aqueous phase was transferred into a fresh tube and 100 μL of each sample was pooled to make quality controls. Samples and quality controls (80 μL) were aliquoted and dried in a speed vacuum at 37 °C and repeated 5 times. Methoxyamine hydrochloride (20 μL; 30 mg/mL in pyridine, and 20 μL of BSTFA + 1% TMCS (Thermo Fisher Scientific, Waltham, USA) were used to derivatize the samples.

2.4. ^{13}C targeted metabolomics

Targeted metabolomics was performed using gas chromatography mass spectrometry (GC–MS). An Agilent 7890 GC system, VF-5 capillary column with 10 m inert eziguard (J&W Scientific, 30 m, 250 μm inner diameter, 0.25 μm film thickness) and an Agilent 5975 MSD (Agilent Technologies, Santa Clara, USA) in electron ionization (EI) mode was used. ^{13}C glucose derived carbon labelling was determined in key metabolites of the glycolytic and TCA cycle via mass isotopomer peak shift analysis. Specific details of the elution time for each intermediate as well as the fragmentation pattern can be provided on request and can also be found on the NIST database.

2.5. Plasma ^{13}C-metabolite enrichment analysis

To determine plasma [U-^{13}C]-metabolite enrichment, 2 μL of plasma was deproteinated by addition of 50 μL of ice cold methanol. After thorough mixing the samples were centrifuged, the supernatant dried, and derivatized as described above. The ^{13}C enrichment in the methoxime TMS derivatives was analysed by selected ion monitoring of glucose (319–323m/z), lactate (219–222m/z), alanine (218–221m/z), palmitate (313–329m/z) and stearate (341–359m/z) ions in EI mode. The metabolite enrichment was expressed as atomic percent excess (APE).

2.6. Metabolomic data analysis

Having extracted enriched and unenriched metabolite abundances using Agilent Mass Hunter Quantitative analysis software, Mass Isotopomer Distribution Vectors (MIDVs) were calculated for each fragment [6]. This removes naturally occurring background isotopic labelling from the fragments. The fractional labelling or APE in each case was determined by the following equation:

$$\mathrm{APE} = \frac{\sum_{i=0}^{n} i \cdot m_i}{n \cdot \sum_{i=0}^{n} m_i}$$

where n represents the number of carbon atoms in the considered fragment and i the mass isotopomers (abundance of M + 0, M + 1, M + 2…etc.). Thus, the APE not only takes into account what proportion of the specific metabolite pool is labelled with ^{13}C, but also the number of ^{13}C atoms incorporated into that specific molecule [7]. The mass isotopomer distribution (MID) is presented as fractional abundance and shows the fraction of the entire specific metabolite pool that is labelled with the exact number of ^{13}C atoms, e.g. M + 2 of 0.2 for citrate means that 20% of all the citrate molecules are labelled with two ^{13}C atoms, while M + 0 of 0.7 means that 70% of the citrate pool contains no ^{13}C atoms (unlabelled). The sum of all MIDs always is equal to one, hence the term fractional abundance. All the above calculations and corrections were calculated by software designed in-house at Metabolomics Australia based on the theory of Nanchen et al. [6].

2.7. Statistical analysis

All data are presented as mean ± standard error of the mean (SEM). Unpaired Student's t-test and factorial ANOVA were used. For the ANOVA, Newman–Kuels post-hoc tests were used to establish differences between groups. Statistical significance was set at $P < 0.05$.

3. Results and discussion

3.1. HFD induced obesity, insulin resistance and glucose intolerance

As expected, body mass was elevated in mice fed the HFD (Fig. 1A). Glucose tolerance was assessed following administration of [U-^{13}C] glucose, allowing us to track the movement of glucose derived carbon through pathways of intermediary metabolism in

muscle via GC–MS. Blood glucose (Fig. 1B) and plasma insulin (Fig. 1C) were higher in HFD mice under fasting conditions, at 15 and 60 min after glucose administration, confirming the presence glucose intolerance and insulin resistance. Prior to [U-^{13}C] glucose administration, no ^{13}C glucose was present in the plasma, whereas 15 min post-gavage ^{13}C enrichment markedly increased (Fig. 1D). After 60 min, there was a reduction in plasma ^{13}C glucose enrichment from 15 min (Fig. 1D), indicating that endogenous unlabelled glucose produced by the liver and/or kidneys diluted the ^{13}C glucose tracer. Importantly, there was no significant difference in plasma glucose enrichment between chow and HFD mice (Fig. 1D). In these experiments, where 99% enriched [U-^{13}C] glucose was administered *in vivo*, all of the normal physiological and biochemical processes related to glucose metabolism including metabolite recycling takes place. It is therefore inevitable that recycling of glucose derived carbon into metabolic by-products such as lactate (Cori cycle) and alanine occurs (glucose–alanine cycle). Since these metabolites could be taken up by muscle to feed into the TCA cycle, tissue metabolite enrichments, particularly at the 60 min time point, may not be entirely derived from plasma ^{13}C glucose. Accordingly, we measured the ^{13}C enrichment of plasma lactate, alanine as well as the free fatty acids palmitate and stearate (Fig. 2A–D). There was a progressive increase in ^{13}C enrichment of lactate and alanine over time, with lactate enrichment being significantly lower in the HFD mice. A similar trend was found with alanine ($P = 0.10$). The reduction in plasma ^{13}C lactate enrichment implies that whole body glucose disposal/glycolysis was reduced in HFD mice, consistent with the fact that these mice have impaired glucose tolerance (Fig. 1B). The data also show that a significant portion of ingested glucose ends up in plasma lactate and alanine, with mice having ~30% and ~20% of the plasma lactate and alanine pools labelled with glucose derived ^{13}C after 60 min, respectively (Fig. 2A and B). In contrast, we could not detect ^{13}C labelling in plasma palmitate or stearate (Fig. 2C and D), indicating adipose tissue *de novo* fatty acid synthesis, at least in the short term, was not making any appreciable contribution to glucose disposal. Therefore ^{13}C labelling in tissue metabolites is not likely to be derived from fatty acids.

3.2. Metabolic flux profiling

Metabolic flux profiling was determined by examining ^{13}C isotope labelling in glycolytic and TCA cycle metabolites in muscle following [U-^{13}C] glucose administration. The basis of this approach is illustrated in the chromatograms in Fig. 3A. Fig. 3A shows lactate labelling 15 min after administration of water (i.e. unlabelled control). Only naturally occurring background isotopic abundance was detected, depicted by the large M + 0 unlabelled isotopomer and corresponding low abundance of the M + 1 and M + 2 isotopomers. Fig. 3B illustrates lactate labelling 15 min after [U-^{13}C] glucose gavage. Compared with Fig. 3A, there was a marked increase in the abundance of the M + 2 isotopomer, demonstrating orally derived [U-^{13}C] glucose is undergoing glycolysis to form lactate. It is important to note that not all of the glycolytic and TCA cycle intermediates could be measured, due to a combination of metabolites being present at low concentrations, lack of volatility, or due to degradation upon heat exposure during chromatographic separation (pyruvate, α-ketoglutarate and oxaloacetate). However, due to rapid exchanges of pyruvate with alanine and lactate, α-ketoglutarate with glutamate, and oxaloacetate with aspartate, it is possible to determine the labelling of these metabolites indirectly [7–9]. Furthermore, in interpreting this data, it is important to highlight that tracer dilution methodology is based on the fact that a change in enrichment of the tracer or its metabolites over time can only occur due to dilution by unlabelled tracee, as metabolism does not distinguish between tracer and tracee, such that loss from the metabolite pool does not affect tracer enrichment [7].

To gain insight about the movement of orally-derived [U-^{13}C] glucose into muscle, we initially compared the ^{13}C labelling of the free glucose pool to that of the plasma. As shown in Fig. 2E, the ratio of intracellular to plasma glucose did not differ between chow or HFD mice. Furthermore, the ratio of intracellular to plasma glucose ^{13}C labelling did not change over time and remained close to one (Fig. 2E). The ^{13}C labelling of metabolites in glycolysis and the TCA cycle is shown in Fig. 3C. No significant changes in labelling were detected over time, indicating that muscle persistently utilized plasma glucose for both glycolytic and oxidative metabolism.

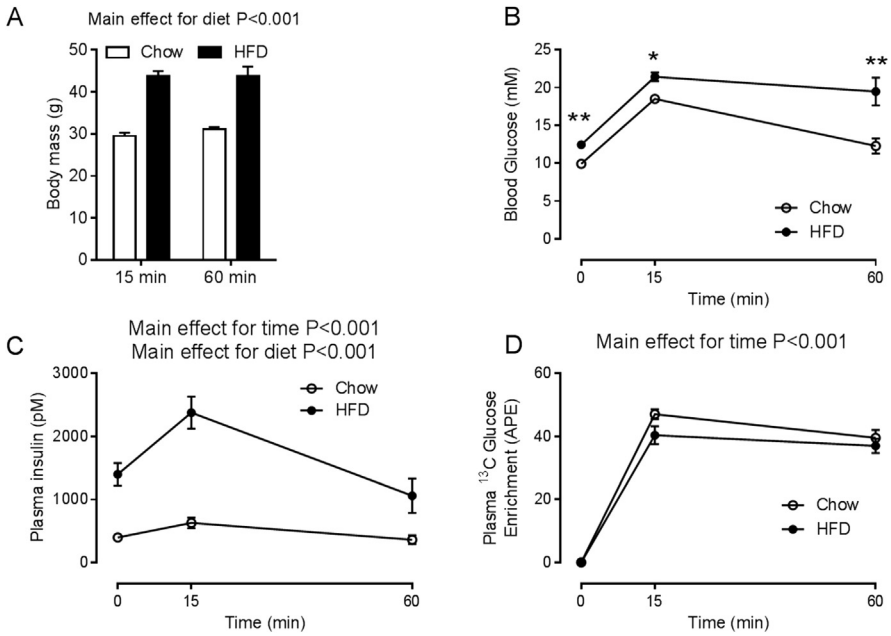

Fig. 1. Effects of HFD feeding on whole-body glucose metabolism. (A) Body mass of mice used in the [U-^{13}C] glucose gavage experiments. (B) Blood glucose; (C) plasma insulin and (D) plasma ^{13}C glucose enrichment. ^{13}C data are expressed as atomic percent excess (APE). For A–D, $N = 10$ chow 15 min, $N = 9$ chow 60 min, $N = 9$ HFD 15 min and $N = 8$ HFD 60 min. Data are mean ± SEM. *$P < 0.05$ vs chow; **$P < 0.001$ vs chow at the indicated times. Data were analysed by two-way ANOVA or two-way repeated measures ANOVA.

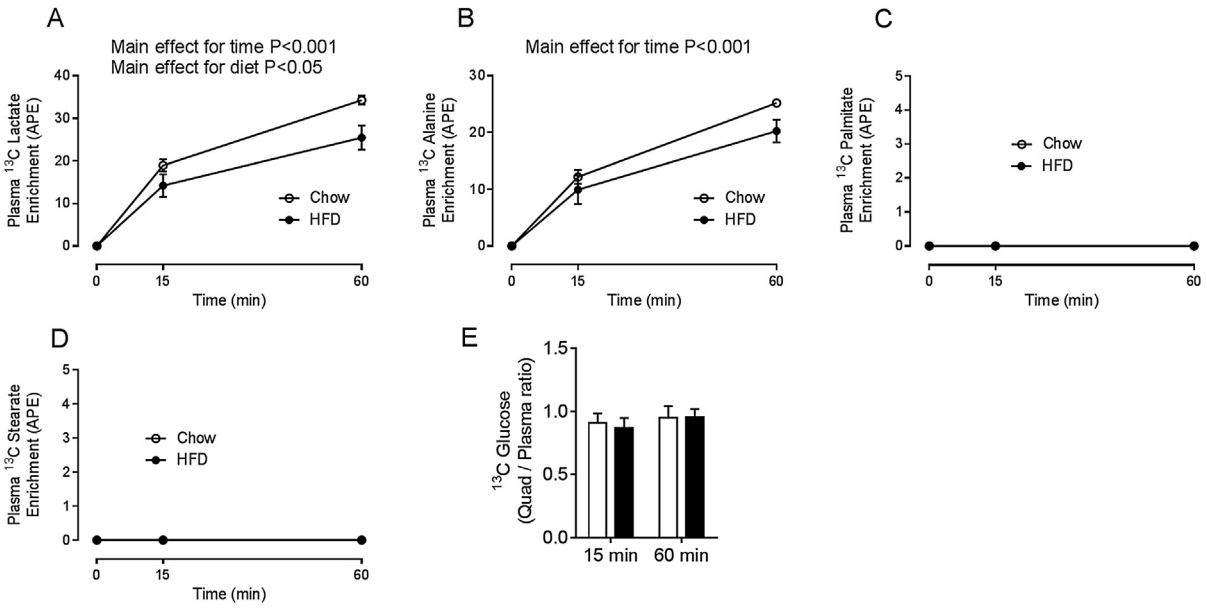

Fig. 2. Plasma ^{13}C metabolite labelling during the OGTT. ^{13}C labelling in plasma (A) lactate, (B) alanine (C) palmitate and (D) stearate. Data are expressed as atomic percent excess (APE). (E) The ratio of ^{13}C labelling between the free intracellular quadriceps and plasma glucose pools. Data are mean ± SEM. $N = 10$ chow 15 min, $N = 9$ chow 60 min, $N = 9$ HFD 15 min and $N = 8$ HFD 60 min. Data were analysed by two-way repeated measures ANOVA.

Although no effects were seen within the glycolytic pathway, significant dietary effects were noted in the TCA cycle. Muscle from HFD mice exhibited a reduction in labelling in all TCA cycle intermediates measured, except for citrate, which remained unaffected (Fig. 3C). The mechanism responsible for this is unclear, but could be due to citrate being exported out of the mitochondria for *de novo* fatty acid synthesis [10,11], such that there is less glucose-derived citrate available for oxidative metabolism. Although liver and adipose are traditionally viewed as the main tissues involved in *de novo* lipogenesis, evidence is emerging that this process does

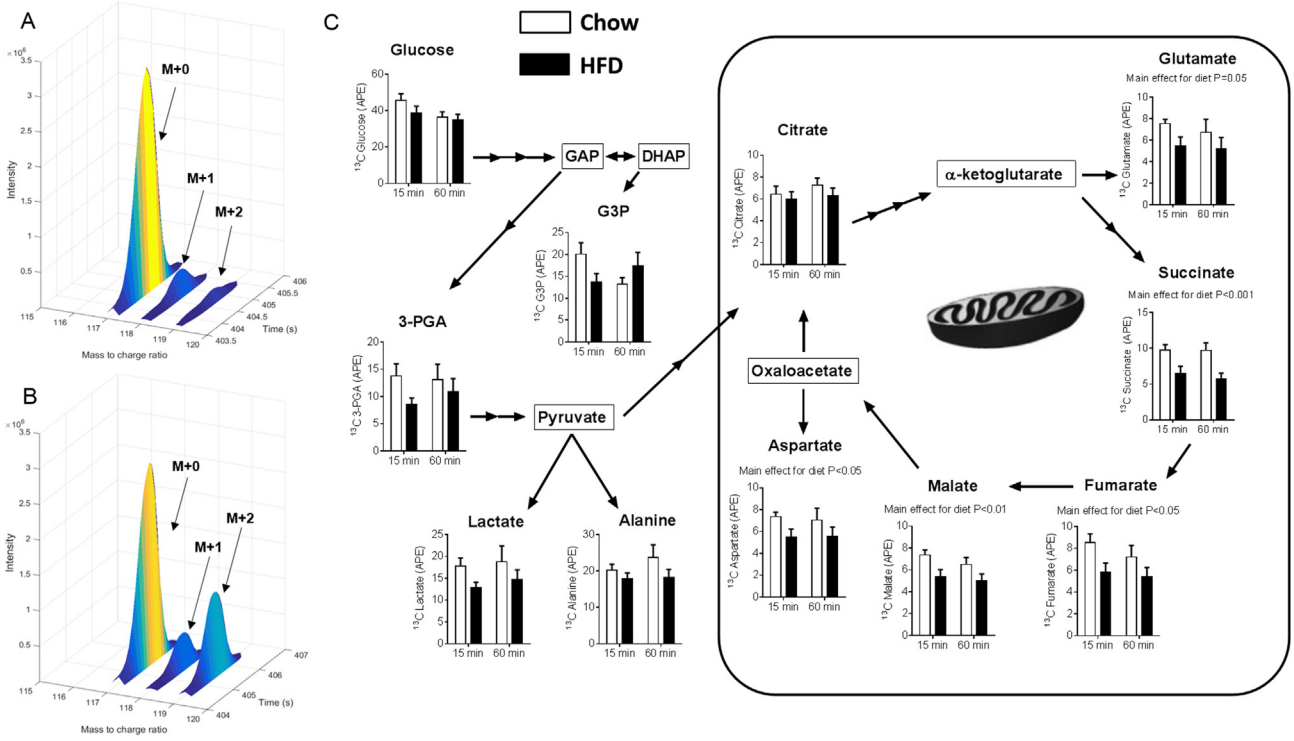

Fig. 3. Dynamic metabolomic profiling of muscle glucose metabolism. (A) Representative chromatogram of quadriceps muscle lactate (117m/z C2–C3 ion) from a mouse 15 min after oral water administration. This demonstrates the natural isotopic background abundance in lactate. (B) Representative chromatogram of quadriceps lactate from a mouse 15 min after receiving a 50 mg oral gavage of [U-^{13}C] glucose. Compared with (A), there is an increase in abundance of the M + 2 (119m/z) isotopomer demonstrating ^{13}C glucose derived carbon in this glycolytic product. (C) Profiling of muscle ^{13}C mass isotopomers in glycolytic and TCA cycle intermediates. Data are expressed as atomic percent excess (APE). Data are mean ± SEM. $N = 10$ chow 15 min, $N = 9$ chow 60 min, $N = 9$ HFD 15 min and $N = 8$ HFD 60 min. Data were analysed by two-way ANOVA. Significance is indicated in each graph. 3PGA; 3-phosphoglycerate, G3P; glycerol 3-phosphate.

occur in muscle [10,11]. Unfortunately, it is difficult to measure *de novo* lipogenesis in the short term with carbon tracers [12], as was the case with these experiments, and thus we could not detect any labelling in triglyceride-derived palmitate or stearate in muscle (data not shown). An alternative explanation for the lack of labelling change in citrate is that labelling of the TCA cycle could be diluted at steps subsequent to citrate. This would most likely occur at the level of α-ketoglutarate/glutamate, as there is already a reduced degree of labelling in glutamate, which is in exchange with α-ketoglutarate (Fig. 3C). The alternate unlabelled carbon sources that could enter the TCA cycle via glutamate and thus dilute labelling beyond citrate could be glutamine, proline, histidine or arginine. Although only speculative, given glutamine is the most abundant free amino acid in muscle and is a commonly used substrate [13], the possibility exists that the HFD increases glutamine catabolism via the TCA cycle, thus resulting in a dilution effect in metabolites below citrate. This is consistent with evidence showing that obese insulin resistant humans [14–16] and rodents [15,17] exhibit altered muscle and whole body protein metabolism. Specifically, in the obese and insulin resistant state, there is resistance to insulin [14] and nutrient [17] induced protein synthesis. Thus, HFD mice may have elevated rates of amino acid oxidation in the muscle during the OGTT. Overall, the data support previous findings of Koves et al. [18] which demonstrate that alterations in muscle mitochondrial glucose oxidation are a key feature of HFD induced metabolic dysregulation in rodents. However, given muscle citrate labelling was unaltered in HFD mice during the OGTT while subsequent TCA cycle metabolite labelling was lower, indicates that this reduction in mitochondrial glucose metabolism does not appear to be mediated by pyruvate dehydrogenase (PDH) inhibition, as has been previously suggested [19–21]. Future work will need to clarify these findings while also deciphering the physiological importance of muscle glucose oxidation in contributing to glucose tolerance. As has been shown in humans [22–24] and in mice [25], muscle glucose oxidation may not be a major contributor to insulin stimulated glucose disposal, thus any defects in this process may not impact on glucose tolerance.

Using the ^{13}C labelling patterns, termed mass isotopomer distributions (MIDs), it was possible to make a qualitative assessment of the pathways by which pyruvate enters the TCA cycle [9]. There are two possible points by which pyruvate can enter the TCA cycle; pyruvate decarboxylation and hence formation of acetyl-CoA via PDH or carboxylation of pyruvate to oxaloacetate by pyruvate carboxylase, known as TCA cycle anaplerosis [9]. The simplified schematic (Fig. 4A) shows the routes of pyruvate entry into the TCA cycle and the expected ^{13}C labelling patterns upon the initial (first turn only) entry of pyruvate. It can be seen that uniformly labelled ^{13}C pyruvate will form M + 2 citrate if acetyl-CoA was generated by PDH. However, if uniformly labelled ^{13}C pyruvate enters the TCA cycle via pyruvate carboxylase, a combination of M + 3 labelled

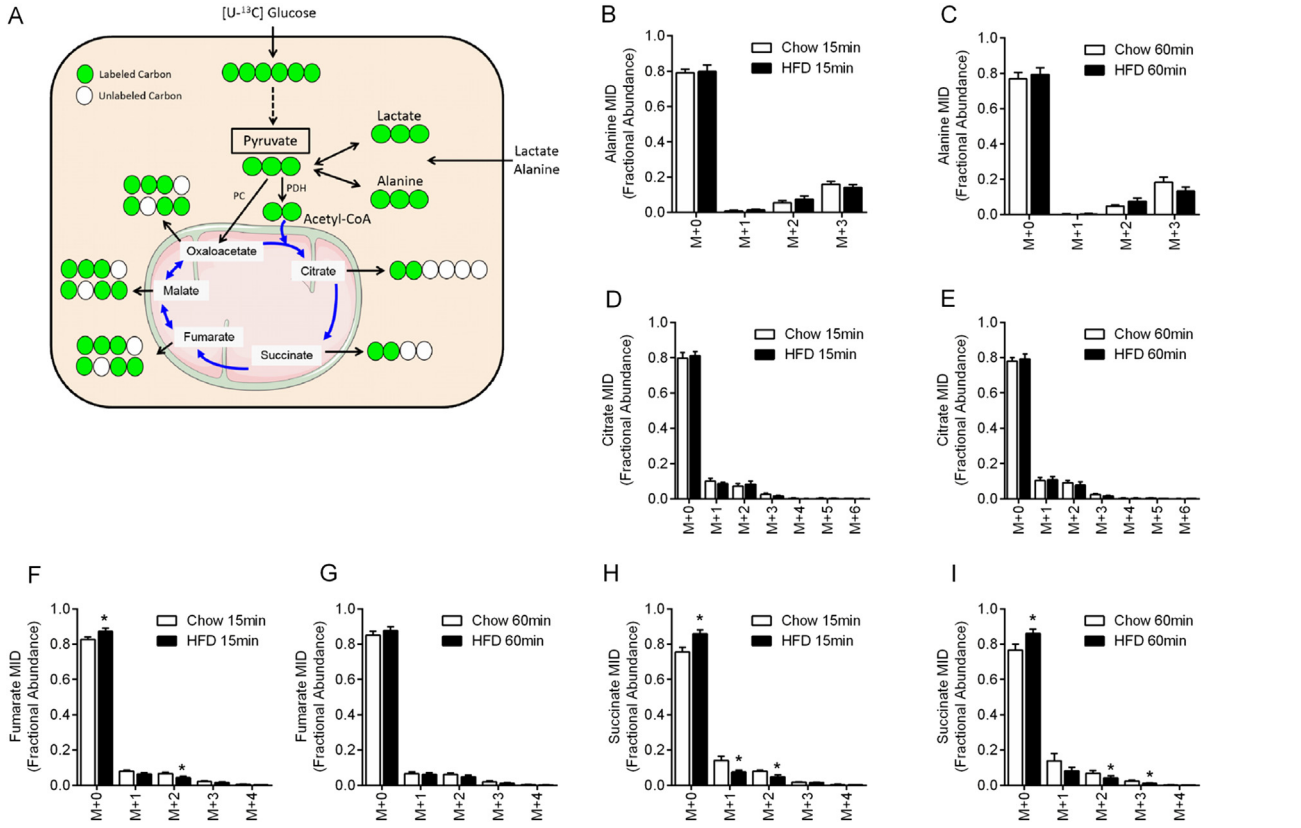

Fig. 4. Skeletal muscle mass isotopomer distributions (MIDs). (A) Represents a simplified schematic of the possible route of glucose derived pyruvate into the TCA cycle and the possible ^{13}C labelling patterns that are produced upon its initial entry (first turn). If [U-^{13}C] glucose derived pyruvate (uniformly labelled ^{13}C pyruvate) enters the TCA cycle via the PDH reaction, carbon 1 is decarboxylated. The resulting ^{13}C labelled acetyl-CoA will condense with unlabelled (M + 0) oxaloacetate thus forming doubly (M + 2) labelled citrate which can then be oxidised, giving rise to downstream products such as M + 2 succinate. If however uniformly labelled ^{13}C pyruvate enters the TCA cycle via carboxylation by pyruvate carboxylase (PD), then triply (M + 3) labelled oxaloacetate will be formed. Due to the exchange and isomerization with the other four carbon intermediates aspartate, malate and fumarate, a combination of M + 3 labelling patterns will occur in these intermediates. (B,C) Mass isotopomer distributions (MIDs) of muscle alanine, (D,E) citrate, (F,G) fumarate and (H,I) succinate. All metabolites in this figure were analysed via their molecular [M − 15] TMS derivatized ions. Data are mean ± SEM and presented as fractional abundance in excess of the natural isotopic background. $N = 10$ chow 15 min, $N = 9$ chow 60 min, $N = 9$ HFD 15 min and $N = 8$ HFD 60 min. Data were analysed by unpaired Student's *t*-test; $^{*}P < 0.05$.

oxaloacetate molecules will be formed [9]. As oxaloacetate is in rapid exchange with the other four carbon TCA cycle intermediates aspartate, malate and fumarate, these will exhibit the same labelling pattern as oxaloacetate, and can therefore be used as an indirect measure of oxaloacetate labelling [7–9]. Thus, if there is substantial anaplerosis, the four carbon TCA cycle intermediates would be expected to exhibit significant M + 3 labelling, and possibly M + 4 labelling due to carryover of acetyl-CoA derived ^{13}C labelling from the PDH reaction. Notably, if there is significant pyruvate anaplerosis the resulting M + 3 labelled oxaloacetate can be further used in the TCA cycle to generate M + 5 citrate, as M + 3 oxaloacetate could combine with M+2 acetyl-CoA [9]. In our experiments, we therefore used the MIDs of alanine (readout of pyruvate), citrate, fumarate and succinate to determine pyruvate entry into the TCA cycle [9]. The MID analysis revealed that 65–70% of labelled alanine/pyruvate is in the M + 3 form (Fig. 4B and C). In the case of citrate (Fig. 4D and E), the majority of labelling occurred in the M + 1 and M + 2 isotopomers, with M + 3 representing only ~10% of the total labelling while M + 5 was not detected, with no effect of diet. The MIDs of fumarate (Fig. 4F and G) revealed that ~12% of total labelling was M + 3, with essentially the same labelling pattern observed in succinate (Fig. 4H and I). Therefore, these data demonstrate that the majority (>95%) of pyruvate must be entering the TCA cycle via PDH.

Finally, it must be acknowledged that the findings presented here only represent relative flux ratios and not absolute flux rates. Determination of absolute metabolic flux rates in tissues during an OGTT represents a significant challenge as neither an isotopic nor metabolic steady state exists. It must also be mentioned that in *in vivo*, unlike *in vitro*, when a large dose of labelled substrate (such as [U-^{13}C] glucose) is administered, the resultant ^{13}C labelling, particularly in the TCA cycle, is quite small. This is a well-known phenomenon that occurs with the use of carbon based metabolic tracers and is explained by the continued metabolism of unlabelled substrates and various isotopic exchanges [7,26].

To the best of our knowledge, we are the first to perform a dynamic ^{13}C metabolomic analysis of intermediary metabolism in skeletal muscle during the physiologically relevant setting of an OGTT. Our findings reveal that there is a consistent defect in glucose derived carbon entering oxidative metabolism in the TCA cycle of skeletal muscle from HFD mice. Finally, we demonstrate that the vast majority of glucose derived pyruvate enters the TCA cycle via PDH, and not through pyruvate carboxylase mediated anaplerosis. These studies pave the way for application of dynamic metabolomic flux profiling approaches to examine metabolism under physiologically relevant conditions *in vivo* and may offer greater insight into mechanisms of disease development.

Sources of funding

This work was supported by a grant from the Diabetes Australia Research Trust. MJM is supported by a fellowship from the National Health and Medical Research Council (APP1059530).

Conflict of interest

None.

Transparency document

Transparency document related to this article can be found online at http://dx.doi.org/10.1016/j.bbrc.2015.04.096.

References

[1] R.A. DeFronzo, Pathogenesis of type 2 diabetes mellitus, Med. Clin. North Am. 88 (4) (2004) 787–835 ix.
[2] S. Andrikopoulos, et al., Evaluating the glucose tolerance test in mice, Am. J. Physiol. Endocrinol. Metab. 295 (6) (2008) E1323–E1332.
[3] J.E. Ayala, et al., Considerations in the design of hyperinsulinemic-euglycemic clamps in the conscious mouse, Diabetes 55 (2) (2006) 390–397.
[4] N. Turner, et al., Distinct patterns of tissue-specific lipid accumulation during the induction of insulin resistance in mice by high-fat feeding, Diabetologia 56 (7) (2013) 1638–1648.
[5] G.M. Kowalski, C.R. Bruce, The regulation of glucose metabolism: implications and considerations for the assessment of glucose homeostasis in rodents, Am. J. Physiol. Endocrinol. Metab. 307 (10) (2014) E859–E871.
[6] A. Nanchen, T. Fuhrer, U. Sauer, Determination of metabolic flux ratios from 13C-experiments and gas chromatography-mass spectrometry data: protocol and principles, Methods Mol. Biol. 358 (2007) 177–197.
[7] R.R. Wolfe, D.L. Chinkes, Isotope Tracers in Metabolic Research: Principles and Practice of Kinetic Analysis, second ed., Wiley-Liss, Hoboken, NJ, 2005.
[8] U. Sauer, Metabolic networks in motion: ^{13}C-based flux analysis, Mol. Syst. Biol. 2 (2006) 62.
[9] J.M. Buescher, et al., A roadmap for interpreting C metabolite labeling patterns from cells, Curr. Opin. Biotechnol. 34C (2015) 189–201.
[10] A.G. Dulloo, et al., Substrate cycling between de novo lipogenesis and lipid oxidation: a thermogenic mechanism against skeletal muscle lipotoxicity and glucolipotoxicity, Int. J. Obes. Relat. Metab. Disord. 28 (Suppl. 4) (2004) S29–S37.
[11] K. Funai, et al., Muscle lipogenesis balances insulin sensitivity and strength through calcium signaling, J. Clin. Invest. 123 (3) (2013) 1229–1240.
[12] M.K. Hellerstein, De novo lipogenesis in humans: metabolic and regulatory aspects, Eur. J. Clin. Nutr. 1 (53 Suppl) (1999) S53–S65.
[13] J.M. Lacey, D.W. Wilmore, Is glutamine a conditionally essential amino acid? Nutr. Rev. 48 (8) (1990) 297–309.
[14] S. Chevalier, et al., The greater contribution of gluconeogenesis to glucose production in obesity is related to increased whole-body protein catabolism, Diabetes 55 (3) (2006) 675–681.
[15] C.B. Newgard, et al., A branched-chain amino acid-related metabolic signature that differentiates obese and lean humans and contributes to insulin resistance, Cell Metab. 9 (4) (2009) 311–326.
[16] N.D. Palmer, et al., Metabolomic profile associated with insulin resistance and conversion to diabetes in the insulin resistance atherosclerosis study, J. Clin. Endocrinol. Metab. 100 (3) (2015) E463–E468.
[17] S.R. Anderson, et al., Diet-induced obesity alters protein synthesis: tissue-specific effects in fasted versus fed mice, Metabolism 57 (3) (2008) 347–354.
[18] T.R. Koves, et al., Mitochondrial overload and incomplete fatty acid oxidation contribute to skeletal muscle insulin resistance, Cell Metab. 7 (1) (2008) 45–56.
[19] M.J. Holness, et al., Targeted upregulation of pyruvate dehydrogenase kinase (PDK)-4 in slow-twitch skeletal muscle underlies the stable modification of the regulatory characteristics of PDK induced by high-fat feeding, Diabetes 49 (5) (2000) 775–781.
[20] B. Hwang, N.H. Jeoung, R.A. Harris, Pyruvate dehydrogenase kinase isoenzyme 4 (PDHK4) deficiency attenuates the long-term negative effects of a high-saturated fat diet, Biochem. J. 423 (2) (2009) 243–252.
[21] P.J. Randle, et al., The glucose fatty-acid cycle. Its role in insulin sensitivity and the metabolic disturbances of diabetes mellitus, Lancet 1 (7285) (1963) 785–789.
[22] J. Rousselle, et al., Relationship between glucose oxidation and glucose tolerance in man, Metabolism 31 (9) (1982) 866–870.
[23] R. Andres, et al., Effect of insulin on carbohydrate metabolism and on potassium in the forearm of man, J. Clin. Invest. 41 (1962) 108–115.
[24] D. Rabinowitz, K.L. Zierler, Forearm metabolism in obesity and its response to intra-arterial insulin. Characterization of insulin resistance and evidence for adaptive hyperinsulinism, J. Clin. Invest. 41 (1962) 2173–2181.
[25] Y. Rahimi, et al., Genetic activation of pyruvate dehydrogenase alters oxidative substrate selection to induce skeletal muscle insulin resistance, Proc. Natl. Acad. Sci. U. S. A. 111 (46) (2014) 16508–16513.
[26] S.F. Previs, H. Brunengraber, Methods for measuring gluconeogenesis in vivo, Curr. Opin. Clin. Nutr. Metab. Care 1 (5) (1998) 461–465.